A Surface Mooring for Air–Sea Interaction Research in the Gulf Stream. Part I: Mooring Design and Instrumentation

ROBERT A. WELLER, SEBASTIEN P. BIGORRE, JEFFREY LORD, AND JONATHAN D. WARE

Woods Hole Oceanographic Institution, Woods Hole, Massachusetts

JAMES B. EDSON

University of Connecticut, Storrs, Connecticut

(Manuscript received 27 March 2012, in final form 24 April 2012)

ABSTRACT

The design of a surface mooring for deployment in the Gulf Stream in the Mid-Atlantic Bight is described. The authors' goals were to observe the surface meteorology; upper-ocean variability; and air–sea exchanges of heat, freshwater, and momentum in and near the Gulf Stream during two successive 1-yr deployments. Of particular interest was quantifying these air–sea fluxes during wintertime events that carry cold, dry air from the land over the Gulf Stream. Historical current data and information about the surface waves were used to guide the design of the surface mooring. The surface buoy provided the platform for both bulk meteorological sensors and a direct covariance flux system. Redundancy in the meteorological sensors proved to be a largely successful strategy to obtain complete time series. Oceanographic instrumentation was limited in size by considerations of drag; and two current meters, three temperature–salinity recorders, and 15 temperature recorders were deployed. Deployment from a single-screw vessel in the Gulf Stream required a controlled-drift stern first over the anchor sites. The first deployment lasted the planned full year. The second deployment ended after 3 months when the mooring was cut by unknown means at a depth of about 3000 m. The mooring was at times in the core of the Gulf Stream, and a peak surface current of over 2.7 m s^{-1} was observed. The 15-month records of surface meteorology and air–sea fluxes captured the seasonal variability as well as several cold-air outbreaks; the peak observed heat loss was in excess of 1400 W m^{-2}.

1. Introduction

Large air–sea heat fluxes are known to be associated with wintertime flow of cold, dry continental air from land over warm western boundary currents. In spite of the interest in quantifying these fluxes and developing a better understanding of the air–sea interactions in western boundary current regions (Cronin et al. 2010), obtaining sustained in situ observations in the upper ocean and at the sea surface has proven to be a challenge, and significant uncertainties about the magnitude and variability of these fluxes have persisted (Moore and Renfrew 2002). Recently, new observations have been obtained in order to reduce these uncertainties and improve understanding of surface meteorology and air–sea fluxes in western boundary current regions. Kubota et al. (2008) and Konda et al. (2010) have reported their observations from surface buoys in the Kuroshio region. Our effort has been to develop a surface mooring capable of providing time series of surface meteorology; air–sea exchanges of heat, freshwater, and momentum; and upper-ocean variability from a site in the Mid-Atlantic Bight that is at times within the core of the Gulf Stream. In this paper we present our approach to designing and instrumenting the mooring and the basic data resulting from the two deployments. In Bigorre et al. (2012, manuscript submitted to *J. Atmos. Oceanic Technol.*, hereafter Part II) we discuss in more depth the air–sea fluxes computed from the observations and investigate the uncertainties in the data, including how they impact the accuracies of the air–sea fluxes.

One of the consequences of strong buoyancy flux both at and east of the Gulf Stream is the transformation of surface water that leads to 18°C Water (EDW) formation. In 2005–07, the Climate Variability and

Corresponding author address: Robert A. Weller, Clark 204a MS 29, Woods Hole Oceanographic Institution, Woods Hole, MA 02543.
E-mail: rweller@whoi.edu

DOI: 10.1175/JTECH-D-12-00060.1

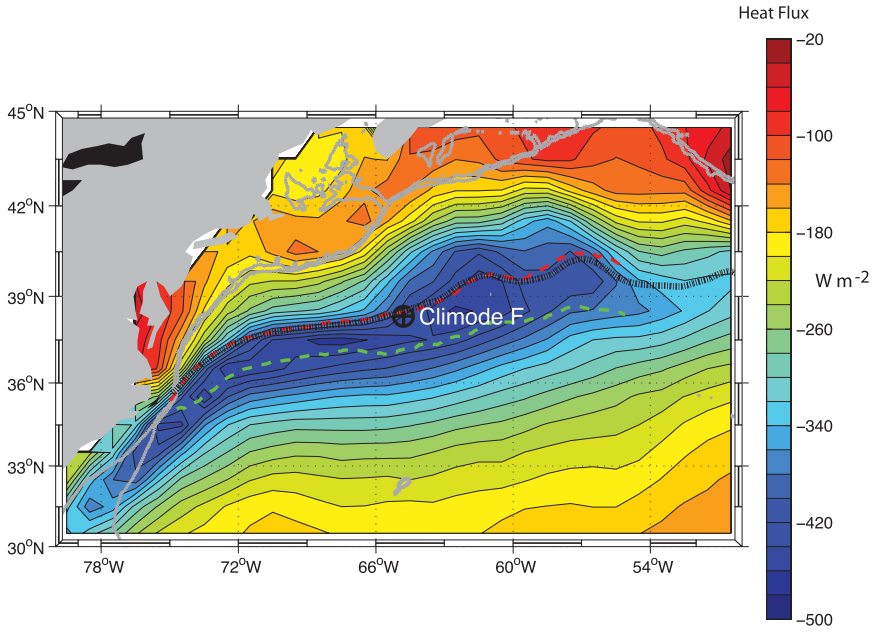

FIG. 1. Map of the Gulf Stream region off the northeastern United States. The bottom bathymetry contours are shown in thick gray lines (200 and 1000 m). Color contours are the winter (December–March) mean of net air–sea heat loss from sensible and latent heat from the Objectively Analyzed Ocean–Sea Fluxes for the Global Oceans (OAFlux; Yu et al. 2004) for the winters of 2005 through 2007. The average location of the north (red dashed line) [south (green dashed line)] wall of the Gulf Stream is indicated, based on the Navy front and eddy analysis product. The average 18°C SST isotherm for the same period is shown (dashed black line). The site chosen for the mooring, 38°N, 65°W, is also shown (black crossed circle).

Predictability (CLIVAR) Mode Water Dynamics Experiment (CLIMODE; Marshall et al. 2009) was conducted to investigate the various processes responsible for water mass transformation leading to EDW creation. The mooring described in this paper was our contribution to CLIMODE, because the deployment of the surface mooring was done in order to improve quantification of the air–sea fluxes in the EDW formation region and the resulting surface buoyancy loss.

To provide an accurate in situ record of the air–sea heat flux we sought to deploy a surface mooring for 2 yr at a site close to the climatological maximum in annual air–sea heat flux (Fig. 1). This site is a deep-water site, in depths of about 4500 m, and also a site that would at times be within the core of the Gulf Stream. One goal was to instrument the surface buoy with the meteorological sensors needed to describe the surface meteorology and estimate the air–sea fluxes of heat, freshwater, and momentum by bulk formula methods (Fairall et al. 1996). The buoy was therefore equipped with redundant, calibrated meteorological sensors (e.g., Weller and Anderson 1996). A second goal was to equip the surface buoy with a direct covariance flux system (DCFS; Edson et al. 1998), which would provide direct estimates of air–sea fluxes (momentum and sensible heat). This method provided the ability to examine uncertainties associated with the methodology of air–sea flux estimation and further investigate the parameterizations used in the bulk formula, as well as the performance of the sensors. Though in prior work (Colbo and Weller 2009) we have characterized the uncertainties in buoy meteorological observations and the derived air–sea fluxes in the subtropics, we anticipated greater uncertainties would be seen in the Gulf Stream location. Finally, a third goal was to obtain upper-ocean currents, temperatures, and salinities. A near-surface current was needed to determine the wind velocity relative to the ocean surface velocity. By collecting 2 yr of data we planned to be able to provide a dataset that would describe the observed variability over a wide range of time scales, spanning diurnal to annual, and would improve our estimates of mean, seasonal, synoptic, and maximum air–sea fluxes. This paper reviews the efforts taken to design a surface mooring that would survive at this site and to equip it with the meteorological and oceanographic instrumentation needed to meet the goals.

Section 2 discusses the conditions anticipated at the site and the design of the surface mooring done in

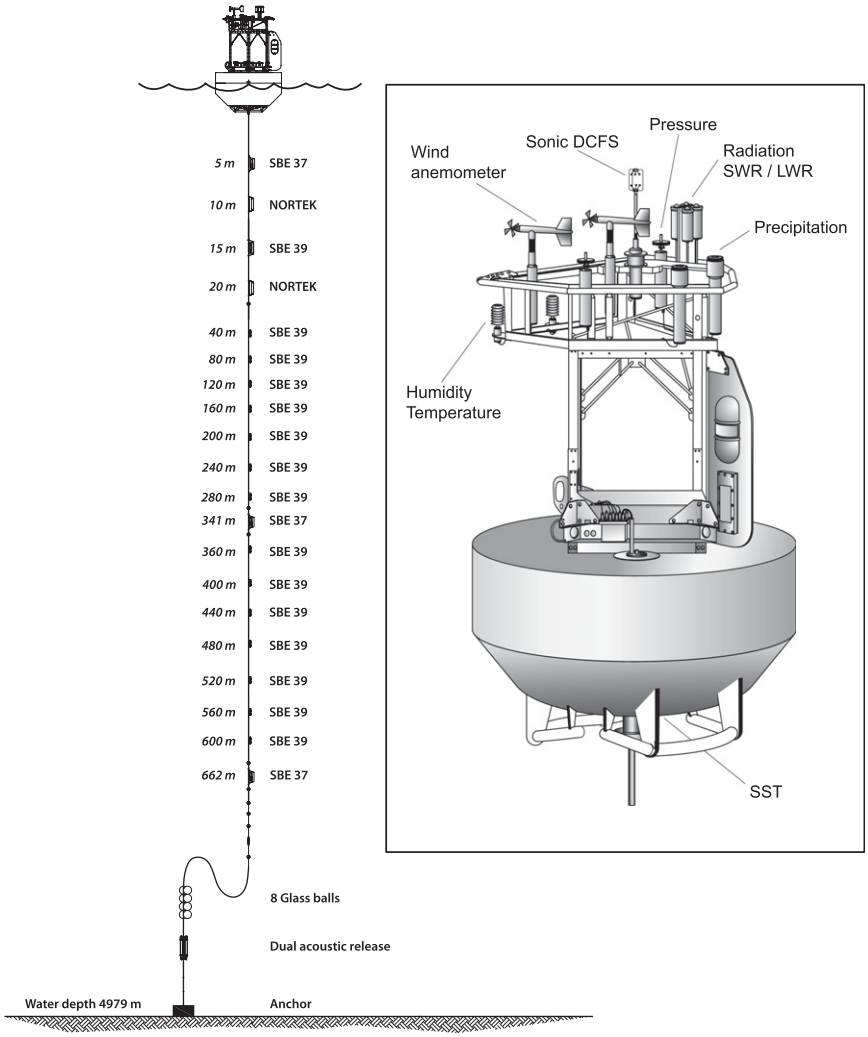

FIG. 2. Schematic diagram of the surface mooring developed for use in the Gulf Stream and anchored near 38°N, 65°W for CLIMODE deployment. The surface buoy carried meteorological instrumentation, dataloggers, and telemetry hardware. The mooring line carried two current meters (Nortek Aquadopps), three SBE 37 temperature and conductivity recorders, and 15 SBE 39 temperature recorders.

response to those conditions. Section 3 describes the meteorological and oceanographic instrumentation sampling and the data return. Section 4 provides an overview of the data that were recovered. Finally, we conclude in section 5 with a discussion and recommendations of further steps that would be taken in a subsequent deployment.

2. Surface mooring design and deployment strategies

A surface mooring (Fig. 2) provided the platform on which to mount meteorological sensors and associated datalogging and telemetry hardware. The 3-m-diameter body of the buoy was made up of Surlyn closed-cell foam. A well in the center of the buoy accommodated an aluminum box in which batteries and dataloggers were located. The superstructure of the buoy provided a location for mounting sensors, a flashing light, a radar reflector, and antennas for data telemetry. A vane was attached to the superstructure in an attempt to orient the buoy relative to the wind and place the relative humidity, air temperature, and wind sensors on the windward side (in order to reduce the heat island effect of the buoy and wind flow distortion by the superstructure). However, it was observed during deployment that this vane, at times, provided insufficient torque to accomplish this steering. Beneath the buoy, the initial plan had been to

install current meters and temperature–salinity and temperature recorders spanning the upper 500 m, using six vector-measuring current meters and 15 temperature or temperature–salinity recorders. Feedback from the mooring design process as discussed below lead to a change in the payload to two smaller Nortek acoustic current meters and 18 temperature and temperature–salinity recorders.

The surface mooring (identified as CLIMODE F, with the first deployment named F1 and the second F2) was to be anchored in 4900 m of water as close as possible to 38°N, 65°W. The strong currents and energetic sea states of the Gulf Stream posed a challenge for the design of the surface mooring. A search of existing velocity observations was used to develop surface-to-bottom ocean current profiles to guide the design work. Both the statics (drag forces of the mean currents) and dynamics (peaks and variability of in-line tensions associated with the surface waves) of the design were considered. The environmental conditions that were used to develop the design of the mooring, the mooring design itself, and the deployment strategies and results are presented here.

a. Gulf Stream velocity profiles and wind and wave conditions

The literature yielded information on Gulf Stream velocities. Joyce et al. (1986) analyzed hydrographic data from CTD sections across the Gulf Stream near 36°N, 72°W and ship's acoustic Doppler current profiler (ADCP) data. Rossby and Zhang (2001) presented ADCP data from multiple crossings of the Gulf Stream at about 37°N, 70°W between 1992 and 1999 by Motor Vessel (M/V) *Oleander* to characterize its near-surface velocity structure. Shay et al. (1995), Bower and Hogg (1996), and Meinen et al. (2009) presented results from current meter moorings and associated data from the Synoptic Ocean Prediction (SYNOP) program. Figure 3 shows along-stream velocity profiles based on these papers. The Gulf Stream currents are concentrated in the upper 1000–1500 m. Because the *Oleander* data showed near-surface flow in excess of 2 m s^{-1}, we considered the possibility of additional wind-driven currents superimposed and chose a surface velocity for the peak current profile of 2.6 m s^{-1}. Then we assumed a decaying profile with depth similar to that reported by Meinen et al. (2009) and Joyce et al. (1986), but did not let the velocity at depth decay below 0.3 m s^{-1}. To provide a margin of safety in the mooring design process, the near-surface flow of the extreme current profile was further enhanced to 3.0 m s^{-1}. For currents reaching the peak current profile, the goal of the mooring design process is to not only survive and not have either the anchor drag or the surface buoy submerge but also have less than 15° departure from vertical at the depths where the instruments are located. Under the extreme current profile, the goal is for the mooring to survive and in-line tensions to remain low enough to allow for a safety factor (the ratio of breaking strength to tension) of 3 or better.

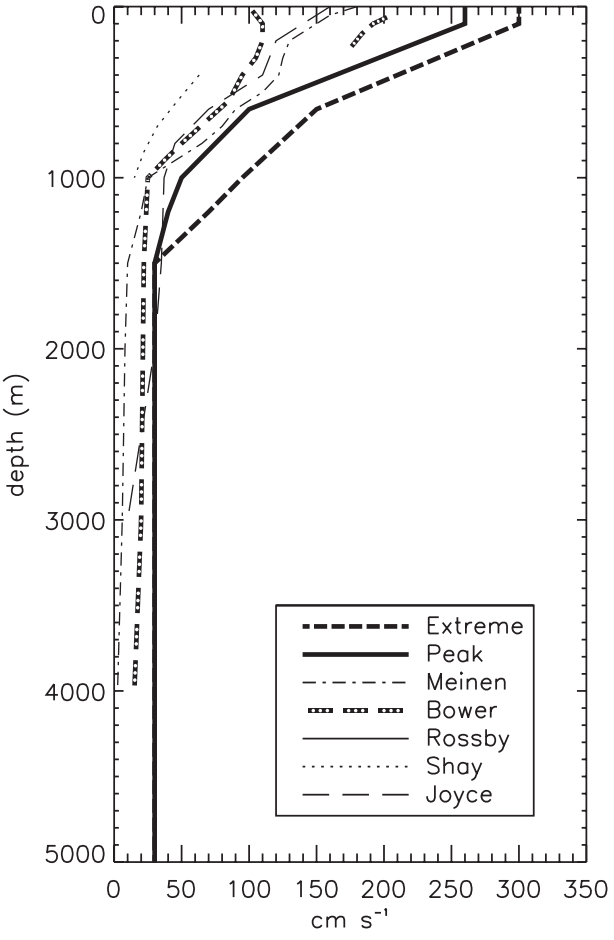

FIG. 3. Gulf Stream velocity profiles developed from literature and the extreme and peak values used for the design of the surface mooring. Peak is the highest current in which we seek to continue to make useful measurements; extreme is the highest current we seek the design to stay on station and not fail. The Joyce profile is developed from Fig. 13 of Joyce et al. (1986), and the Meinen profile is developed from Fig. 9 of Meinen et al. (2009).

In the mooring design process two analyses are done—one is only static and the other is both static and dynamic. The dynamic analysis takes into account the forcing of the surface buoy by surface waves and winds. Data from a National Data Buoy Center (NDBC) buoy east of Cape May, New Jersey (buoy 44004; 38.47°N, 70.56°W), were used to define normal as well as peak and extreme wave conditions. Normal conditions were waves of a 9-s period and 2-m significant wave height, peak conditions were waves of a 9-s period and 4-m

TABLE 1. Tensions (lb) at the top of the anchor and at the base of the buoy under peak and extreme current profiles for three design scenarios—A: 7/16 -in. wire to 640-m depth with fairing, then 3/8 -in. wire to 2000 m; B: 7/16 -in. wire to 1000 m with fairing, then 3/8 -in. wire to 2000 m; and C: 7/16 -in. wire to 1000 m with fairing to 640 m, then 3/8 -in. wire between 1000 and 2000 m. The first number is the tension predicted by SURFMOOR, the second number, if present, is tension predicted by Cable.

	Peak		Extreme	
	Buoy	Anchor	Buoy	Anchor
A	6253	4867	7808	6501
B	6068/6161	4623/4793	7512/7552	6151/6288
C	6382/6469	4929/5099	7958/7981	6585/6713

significant wave height, and extreme conditions were waves of an 11-s period and 12-m significant wave height. For the dynamic analyses, extreme winds of 30 m s^{-1} were used, with normal winds taken as 6 m s^{-1} and peak winds as 12 m s^{-1}. Grosenbaugh (1995) and Schulz et al. (2011) provide more discussion on surface mooring design.

b. Surface mooring design

Two analysis packages were used to do both static and dynamic analyses to guide the design of the mooring. SURFMOOR [an unpublished FORTRAN surface mooring design program developed at Woods Hole Oceanographic Institution (WHOI)] and WHOI Cable (Gobat and Grosenbaugh 2000) are used for static analyses. In the static analysis, we look at the balance of drag forces from the currents, the buoyancy of the surface buoy, the mass of the instruments, the buoyancy of any subsurface flotation, and the mass of the anchor. The additional design challenge of the mooring as a system that is subjected to surface wave orbital velocities as well as mean currents was addressed by using WHOI Cable to examine the static and dynamic performance of different configurations of the mooring and evolve the design toward one that would maximize the chance of survival. In part, this involved altering the mooring design to avoid the possibility of a heave response at surface gravity wave and swell periods. Drag associated with the strong currents was reduced by attaching fairing onto the upper 980 m of the mooring line and by adding to the mooring line only a limited number of small oceanographic sensor packages in the upper 600 m of the water column. Chain is typically used in the upper 50 m both to facilitate recovery and deployment, and also to add mass below the buoy during the initial deployment. However, 50 m of chain made the load beneath the buoy too high; and 20 m of galvanized 3/4-in. chain was used. Below that, plastic-jacketed torque-balanced wire rope was used down to 2000 m for strength and resistance to fish bite. Fairings were clipped on to the wire rope down to a depth of 983 m. Nylon rope (3000 m long) was attached below the wire rope, and 2000 m of polypropylene rope lead down to chain, glass balls, and the anchor. The scope of the mooring (ratio of the length of the mooring to the water depth) was 1.45.

TABLE 2. The safety factor (breaking strength/tension) for various components of potential mooring configurations (A, B, C as in Table 1) under peak and extreme current profiles from the static design analysis. The left two columns under each profile are for the wire rope; the right three columns are for nylon rope.

	Peak					Extreme				
	7/16″	3/8″	7/8″	1″	9/8″	7/16″	3/8″	7/8″	1″	9/8″
A	3.4	2.7	4.2	5.4	4.1	2.7	2.1	3.1	4.0	3.0
B	3.5	3.0	4.4	5.7	4.3	2.8	2.3	3.3	4.2	3.2
C	3.3	2.8	4.1	5.3	4.0	2.6	2.1	3.1	3.9	3.0

In finalizing this design, options for the configuration were explored that included use of 3/8-in.-diameter plastic-jacketed wire rope versus use of 7/16-in.-diameter plastic-jacketed wire rope in the section of the mooring below the chain, as well as the use of clip-on fairings along that wire rope to reduce drag. We also varied the scope of the mooring, examining values of 1.25, 1.35, 1.45, and 1.50. A scope of 1.45 gave the best results. Tables 1 and 2 summarize the key findings. Extending the fairing down to 1000 m reduced tensions and increased the safety factors. Use of the heavier 7/16-in. wire rope in the upper 1000 m yielded better safety factors as well. The 8000-lb. in-water weight of the anchor thus appeared appropriate for the predicted ~6200-lb. tension under option B. For additional safety against dragging, a 40-lb. Danforth anchor was attached to the cast anchor by a 3-m section of chain.

A key concern in the dynamic analysis is how the mooring performs as a system under surface wave forcing. In particular, the Cable program is run to look at the cyclic in-line tensions associated with the surface buoy moving with the surface waves and swell. A mooring with a resonant vertical heave response near surface wave and swell periods would be at risk because of high in-line tensions. Load cycling using a steady wave state in the extreme environment showed a load cycle between 7000 and 9000 lb. When random wave patterns were input (wind waves and swell), load cycles as much as 5500–10 000 lb. in one period were seen. This is unusual, but was considered when selecting components to be used in the mooring. Because of the potential for cyclic fatigue in the extreme environment, we decided to use 7/16-in. wire with fairing down to 1000 m. Using 7/16-in. wire without fairing would have increased the static buoy load in Table 1 (extreme) to over 11 000 lb.

TABLE 3. Deployment and recovery times, anchor locations, and water depths for the CLIMODE surface mooring deployments.

Deployment name	CLIMODE F1	CLIMODE F2
Deployment	2118 UTC 13 Nov 2005	2105 UTC 20 Nov 2006
Recovery	0945 UTC 19 Nov 2006	0945 UTC 9 Feb 2007
Anchor location	38°19.1′N, 64°47.3′W	38°01.6′N, 64°47.5′W
Water depth (m)	4981	4979

c. *Mooring deployment strategies and results*

The target site for the mooring deployment was 38°N, 65°W. The actual anchor sites, shown in Table 3 together with water depths and exact deployment and recovery times, were the result of a combination of time constraints, working conditions, and other factors. Also of concern was the proximity of the New England Seamount chain and submarine cables. Traditionally, we deploy surface moorings by deploying the surface buoy first, followed by the deployment of line and instruments as the ship steams slowly into the wind and current (this way the surface buoys trails aft, keeping the mooring line straight), and progresses toward the intended anchor site at about 1 kt through the water. This slow speed ensures that tensions in the mooring line remain low to minimize the potential for damage to the sensors in the mooring line. After crossing over the anchor site, the anchor is dropped to fall to the seafloor. This approach is not possible in strong currents, however. The buoy needs to be deployed and a way found to get it to stream out away from the ship while the ship moves to the anchor site. In this case, further challenges were encountered when using a single-screw vessel without dynamic positioning in the strong currents of the Gulf Stream. We were embedded in the Gulf Stream during both deployments. The approach taken was to start ~15 nm upstream, pointing the bow into the current, and steaming slowly into the current, allowing the ship to fall back stern first toward the targeted anchor site. With the ship making headway into the current, the current carried the surface buoy, which was first deployed downstream and away from the stern of the ship. At the same time, though, the strong current carried the ship and buoy downstream. However, while working to keep the wire going aft rather than tending too far either port or starboard, we had only limited ability to steer the ship along a desired track line to the anchor site. Thus, when we reached the point where the anchor was ready to be deployed, we checked with the ship's 12-kHz depth sounder to ensure that we were over a region with a relatively flat bottom, in the depth range the mooring was designed for, and away from the seamounts and submarine cables, and we chose to deploy there rather than prolong the work deck and experience further risk to the mooring and instruments as we tried to maneuver.

We did an acoustic survey to establish the location of the anchors each time. F2 was 33 km south of F1 resulting from strong southward currents and ship-handling challenges encountered during its deployment; F1 (F2) was 40 (19) km from 38°N, 65°W. At any given time, the position of the surface buoy was determined by the drag of the currents on the mooring line and the buoy hull in combination with the drag of the surface wind, the position of the surface buoys was tracked using the Argos telemetry transmitter on the buoy, and the average location of the buoy was 5 km from the anchor. At most this displacement was 7 km. The separation was lower than the 5-km mean 60% of the time. Because of predominant southward currents, the buoy was south of the anchor site about 65% of the time during the first-year deployment.

The two 1-yr deployments were planned based on the capacity of the battery packs installed in the buoy and the desire to have freshly calibrated sensors in operation at the beginning of each winter. The first-year deployment was successful, with the mooring staying on the station even though currents as high as 2.4 m s^{-1} were experienced. The second deployment ended shortly after the mooring broke free at around 2300 UTC 31 January 2007; and the surface buoy went adrift, following a meander of the Gulf Stream until it was recovered on 9 February 2007 by Research Vessel (R/V) *Knorr*.

A load cell beneath the buoy reported tension, and observed values were consistent with those predicted during the mooring design process. The load cell data from the second deployment are shown in Fig. 4. From late November to early December 2007, observed surface currents were about 1.5 m s^{-1} and 4000–5000-lb. tensions at the buoy were as expected. The highest observed currents of 2.74 m s^{-1} and a spike in tension at the buoy of up to 7800 lb. were observed at or close to the time of the break in the mooring line on 31 January 2008 when the mooring was in the core of the Gulf Stream, as it had been on 28 January. Upon recovery, the mooring was found to have parted at a depth of about 3000 m in the nylon rope. However, the recovered end of the mooring line was sent out for examination, and the examiners concluded that the line had been cut under high tension rather than having experienced a material failure under load. The 7/8-in. nylon rope had a safety factor (the ratio of breaking strength to tension) of at least 3 for both the predicted and observed peak loads (Table 2).

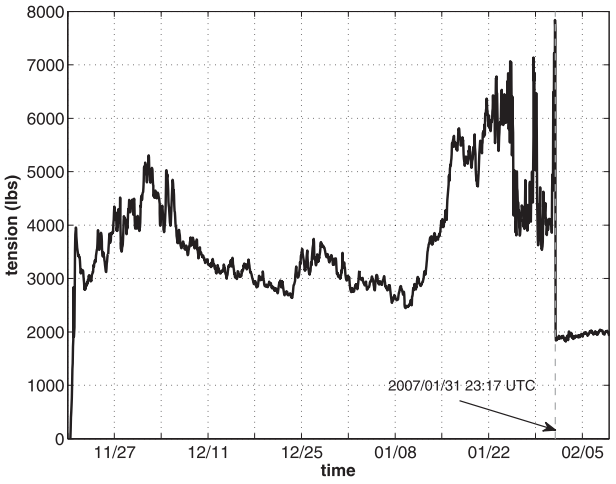

FIG. 4. Time series plot of mean tension at the base of the buoy measured by a load cell located in the buoy bridle. The means are computed as 16-min averages. The mooring was in the core of the Gulf Stream both on 28 and 31 Jan 2008. The drop in tension on 31 Jan coincides with the parting of the nylon rope.

3. Instrumentation, sampling, and data return

The instrumentation deployed on the surface buoy and mooring line, the sampling procedures used, and the success at making the basic observations are summarized here.

a. Mean meteorological sensors

Sensors were mounted to obtain all of the mean meteorological variables used in the bulk formula approach. In anticipation of rough conditions, most sensors were duplicated, though some triplicated. The sensors and sensor heights are summarized in Table 4. Two separate Air–Sea Interaction Meteorological Systems (ASIMET; Hosom et al. 1995) were installed; these include power, datalogging, satellite data telemetry, and the following mean meteorological sensors: wind speed and direction, air humidity and temperature, barometric pressure, rainfall accumulation, incoming longwave and shortwave radiation, and sea surface temperature (SST) from Sea-Bird Electronics SBE 37 temperature–conductivity recorders attached to the bridle beneath the buoy. The meteorological instruments were located between 2.7 and 3.6 m above the mean water line of the buoy, and SST and salinity were sampled at a depth of 0.89 m. The recording rate was once per minute and each data record was typically an average over the minute. Wind was sampled every 5 s, and converted to (u, v) components using compass and vane readings. At the end of the minute, 11 samples were vector averaged and the resulting wind speed and direction were recorded. Another estimate of wind speed is made based on the number of rotations of the anemometer's propeller per unit time. This estimate is therefore a scalar average over 1 min. For directional variables (wind and current headings) to be referenced to true north, the local magnetic deviation was added at postprocessing, using a value of $-16.57°$. Shortwave radiation was sampled every 10 s and averaged over six samples each minute. Hourly averages were computed by the datalogger and relayed via satellite telemetry for monitoring throughout the deployment. A third ASIMET set of sensors (excluding precipitation) was deployed for

TABLE 4. Summary of the mean and turbulent meteorological sensors deployed on the two deployments of the surface mooring, giving the heights of these sensors above the mean waterline of the buoy.

CLIMODE F1			CLIMODE F2		
Observations	Sensor	Height (cm)	Observations	Sensor	Height (cm)
Relative humidity and air temperature	Rotronic MP-100F	273	Relative humidity and air temperature	Rotronic MP-100F	300
Barometric pressure	Heise DXD	325	Barometric pressure	Heise DXD	310
Wind speed and direction	R. M. Young 5103	340.5	Wind speed and direction	R. M. Young 5103 propeller/vane and	356
	Propeller/vane			Gill WindObserver sonic	358
Rain	R. M. Young 50201 siphon gauge	291.5	Rain	R. M. Young 50201 siphon gauge	305
Incoming shortwave	Eppley PSP	348.5	Incoming shortwave	Eppley PSP	353
Incoming longwave	Eppley PIR	348.5	Incoming longwave	Eppley PIR	353
SST	SBE 37	−89	SST	SBE 37	−89
Turbulent wind and temperature	Gill R3–50	406	Turbulent wind and temperature	Gill R3–50	403

redundancy, with the modules recording data internally. The two precipitation sensors were equipped with electric heaters to prevent freezing of the water in the collection volume, and a thermostatic switch provided power to these heaters when air temperature approached or was lower than freezing.

b. Direct covariance flux system

A DCFS (Edson et al. 1998) was deployed to compute fluxes of momentum and buoyancy using the direct covariance (or eddy correlation method). The DCFS was comprised of a three-axis ultrasonic anemometer/thermometer (Gill RS-50) for velocity and ''sonic'' temperature, an inertial sensing system for platform motion (Systron Donner MotionPak II), and a compass for heading (Precision Navigation). The ultrasonic anemometers measure the velocity components from differences in the time of flight of acoustic pulses emitted from three pairs of opposing transducers. The average of these times is used to compute the speed of sound, which can be readily related to the sonic temperature. The inertial sensing system combines three-axis solid-state accelerometers and angular-rate sensors. Filtering and integration of these measurements are used to compute the platform velocities using the approach described by Edson et al. (1998), with improvement described by Miller et al. (2008).

Platform motion is then removed from the sonic velocities after incorporation of the compass to compute the north and east velocity components, and thereby the wind direction. The velocity components are then rotated into the mean wind to compute the along- and crosswind components of the momentum flux. The sonic temperature closely approximates the virtual temperature (Larsen et al. 1993), and its correlation with the vertical velocity provides estimates of the buoyancy flux. The DCFS also provides a record of buoy tilts and heave to estimate the significant wave height.

The motion sensors and compass were sampled and stored at 5 Hz, while the sonic anemometer data were sampled at 20 Hz and averaged to 5 Hz before storage. Because of power limitations the DCFS only sampled for 20 continuous minutes every hour. The stored data were used to compute the fluxes and 1-min means in postprocessing after recovery. Because the filtering process produces end effects (Gibbs phenomenon), the first and last minutes of the data record were discarded, leaving 18-min-long records every hour. The system ran continuously (apart for a couple gaps in data, less than 3 days long) during the first deployment and was replaced with an identical system that also ran continuously during the second deployment. The 18-min averages from the three-axis sonic provided a continuous record of the wind velocity, which was used to fill in gaps in the mean wind record when the mechanical anemometers failed.

c. Oceanographic instrumentation

The mass and drag of in-line oceanographic instrumentation had a significant impact on the performance of various mooring designs that were considered. As a result, only two small, single-point acoustic current meters (Nortek Aquadopps) were deployed near the surface at 10 and 20 m. This was done in order to obtain a near-surface velocity with some redundancy and also to examine near-surface shear. The near-surface velocity was also needed to correct the wind velocity measured on the buoy to wind velocity relative to the sea surface as needed in the bulk flux formula. The near-surface velocity was also of interest to examine the performance of the surface mooring design and to quantify the advection terms of the upper-ocean heat budget. When deployed, the Aquadopps were fitted with vanes to orient the instruments with respect to the flow. These vanes had been provided by Nortek to keep the acoustic beams of the current meters oriented upstream of the mooring line and mounting bar so that the mooring was not distorting the measured flow.

To measure water temperature, 15 Sea-Bird Electronics SBE 39 temperature recorders were deployed; the first was bolted to a load bar made of 6Al-4V titanium and shackled in line with the chain at 15 m. The rest were clamped to the wire rope in the upper 600 m. Three additional SBE 37 instruments recorded temperature and conductivity; the deepest one (662 m) also recorded pressure. These were bolted to load bars made of flat 6Al-4V titanium plate that in turn were shackled to sections of the $^{7}/_{16}$-in. wire rope. The Sea-Bird instruments recorded data every 5 min. Finally, two SBE 37 instruments were attached next to each other, on the bridle under the buoy, as part of the two ASIMET systems and provided estimates of SST and conductivity. Table 5 summarizes the configuration of the subsurface oceanographic instrumentation.

d. Data return

Several instruments failed on the buoy during the first-year deployment. Damage to the buoy superstructure and paint left behind on the buoy suggest that the buoy was hit by a ship, in spite of its flashing light and radar reflector. Several anomalies in the data record indicate that this collision occurred around 0830 UTC 19 January 2006 when, as a consequence, the R. M. Young propeller vane anemometers were damaged and lost their vanes. On 12 April 2006, the damaged sensors were replaced. On 12 September 2006, as Extratropical Storm Florence

TABLE 5. Subsurface oceanographic instrumentation under CLIMODE F surface mooring.

Sensor	Variables	Depth (m)	Record interval (min)
SBE 37 (2)	*T* and *C*	0.89	1
SBE 37	*T* and *C*	5	5
Nortek Aquadopp	*U*, *V*, *W*, *T*, and *P*	10	15
SBE 39	*T*	15	5
Nortek Aquadopp	*U*, *V*, *W*, *T*, and *P*	20	15
SBE 39	*T*	40	5
SBE 39	*T*	80	5
SBE 39	*T*	120	5
SBE 39	*T*	160	5
SBE 39	*T*	200	5
SBE 39	*T*	240	5
SBE 39	*T*	280	5
SBE 37	*C* and *T*	341	5
SBE 39	*T*	360	5
SBE 39	*T*	400	5
SBE 39	*T*	440	5
SBE 39	*T*	480	5
SBE 39	*T*	520	5
SBE 39	*T*	560	5
SBE 39	*T*	600	5
SBE 37	*C*, *T*, and *P*	662	5

passed near the buoy, the R. M. Young anemometers stopped recording wind speed and only wind direction was later available from these sensors. Upon recovery of the buoy, it was found that the anemometers had broken propeller shafts, which may have been caused by wave impacts. Consequently, one two-axis sonic sensor (Gill WindObserver II) was installed in place of one R. M. Young propeller-vane anemometer for the second deployment. This sonic sensor reliably returned wind speeds, but a software problem rendered the compass reading inaccurate.

The most meteorologically reliable sensors were SST and incoming shortwave radiation, with data returns for both primary sensors higher than 99%. One barometer had a 95% data return while all incoming longwave radiation sensors were 85% or higher. For relative humidity and air temperature one instrument out of the two primary sensors had a data return of 99% and 97%, respectively, but other sensors failed prematurely. Wind sensors had multiple failures during CLIMODE 1, but the best instrument had a data return of 97% or higher (not including the period after damage from Florence). The wind and humidity sensors proved more fragile overall, but instrument redundancy supported development of a 15-month record. The best rain gauge on CLIMODE 1 had 60% data return only. Upon recovery, corrosion was observed in the electronic components of the precipitation gauges. For 254 out of 453 days of the 15 months, the rain gauges provided the rain data. As discussed in Part II the rain gauge data compared well with European Centre for Medium-Range Weather Forecasts (ECMWF) high-resolution forecast model rain rates, and gaps in the rain data were replaced with the hourly ECMWF values linearly interpolated to 1-min resolution.

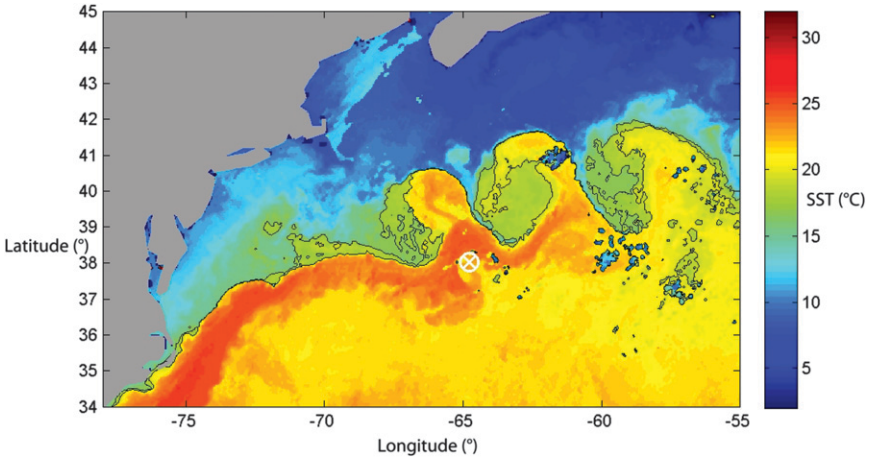

FIG. 5. A 3-day composite Advanced Very High Resolution Radiometer (AVHRR)-based SST field for 9 Jan 2007. The location of the surface mooring is shown (white circled cross). The 17° and 19°C isotherms are denoted (black contours). The blue patches inside the warm meanders are probably warm clouds. A nine-point median filter is applied to the original AVHRR image data. [Adapted from image from a Johns Hopkins University Applied Physics Laboratory Ocean Remote Sensing Group image.]

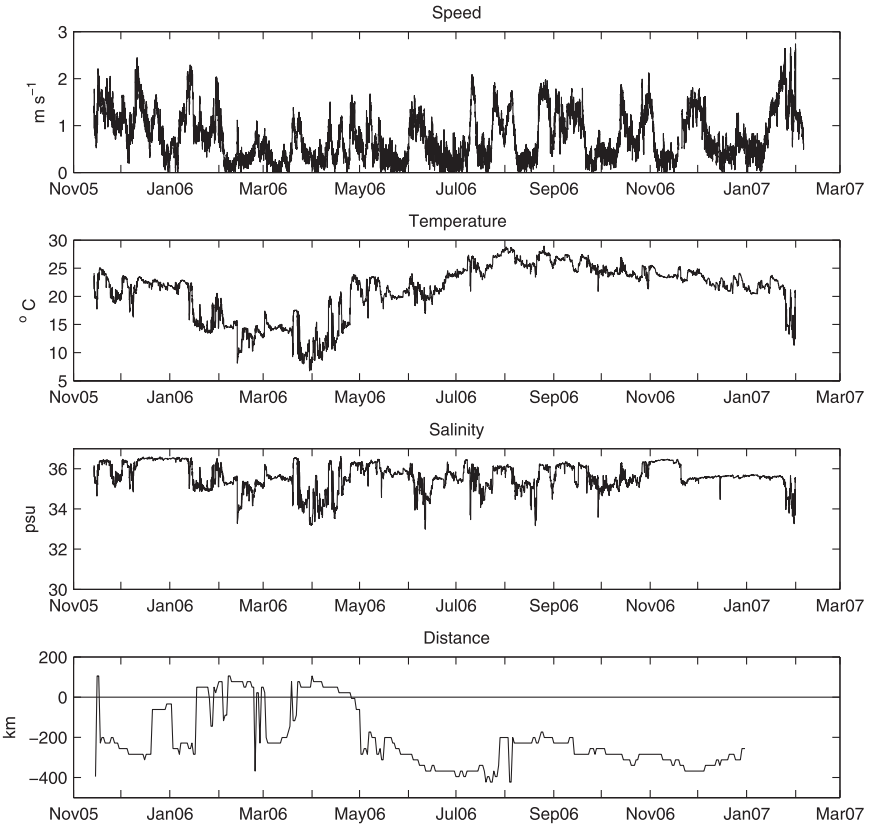

FIG. 6. (from top to bottom) Current speed, sea surface temperature, sea surface salinity, and meridional separation between the surface buoy and the north wall of the Gulf Stream. The buoy was north of the north wall in the later part of January–February 2006 and again in March and April 2006.

The oceanographic instruments had good data return. All SBE 39 instruments provided full records (except for SBE 39 at 15-m depth on CLIMODE 2, which was lost on recovery). The two SBE 37 instruments at 5- and 660-m depths had a complete temperature record (as well as conductivity for the deeper one). The SBE 37 at 341-m depth had periods with noisy data and suspicious offsets compared to nearby instruments, so its temperature data return was 76% only (its conductivity cell failed after a few hours). The two Aquadopp current meters on the mooring line returned full records. However, on CLIMODE 1, their vanes broke a few days after deployment. Comparison with available ADCP data from the ship at recovery showed good agreement. Also, diagnostic data from the Aquadoppps (a 1-Hz return for 1 min every 12 h) showed no high-frequency signal coming from either flow distortion or mooring vibration, which could have impacted the measurements. On CLIMODE 2, two ad hoc vanes were made of 1-in. Plexiglas and ¼-in.-thick Delrin, which were installed on the current meters at 10 and 20 m, respectively, and operated normally until recovery (Tupper et al. 2008).

4. Overview of the observations

In this section we use this first moored time series of surface meteorology and upper-ocean variability at a Gulf Stream location off the northeastern United States to provide an indication of the extent to which the surface mooring succeeded in meeting our goals. The mooring location was well chosen from the perspective that it was within the Gulf Stream on a number of occasions (Fig. 5). At the same time, the location is one where the Gulf Stream meanders and moves north and south of the mooring site, so that sampling was done at times in waters north of the Gulf Stream (Fig. 6). The oceanographic observations are discussed first, followed by the bulk meteorological observations. The air–sea bulk formula fluxes are also presented. Part II provides discussion of observational uncertainties and of comparisons between the bulk formula and DCFS fluxes.

a. Oceanographic observations

Because the mooring sampled north of the Gulf Stream, in, and south of the Gulf Stream, the observed

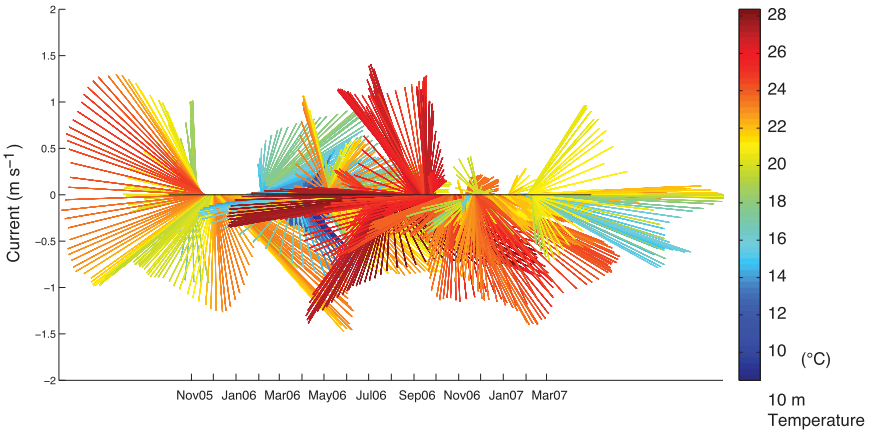

FIG. 7. The 10-m-deep currents shown as vectors, 15-min data averaged to 6-h values, and then smoothed over 2.5 days. Vector color is the temperature at 10 m (color bar: °C).

velocity and temperatures varied greatly. Figure 7 shows the smoothed 10-m velocity vectors that are color coded by 10-m water temperature, and Fig. 8 shows the 18 temperatures from the moored instruments contoured as a function of distance along the mooring line. The mixed layer depth is also shown. Strong flows were observed toward all compass headings resulting from the meandering structure of the Gulf Stream in the region. The maximum 10-m velocity recorded during the first deployment was 2.54 m s^{-1}; the mean for 10 m for the first (second) deployment was 0.74 (0.82) m s^{-1}. The overall maximum speed at 10-m depth was 2.74 m s^{-1} and was observed close to the end of the second deployment; at this time the buoy was on the warm side of the north wall, near the high-velocity core of the Gulf Stream.

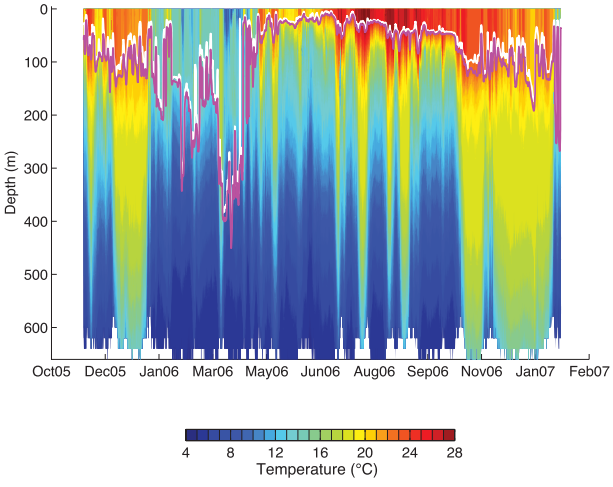

FIG. 8. Hourly temperature as a function of distance along the mooring line, with estimates of the depth of the mixed layer [0.5°C down from SST (white) and 1.0°C down from SST (magenta)].

b. *Mean meteorological observations*

Statistics of wind speed and direction are summarized, along with statistics from all mean meteorological observables, in Table 6. The hourly averaged wind speed and direction time series are shown in Fig. 9, with additional running mean low-pass filters of 1 and 4 days applied. There was considerable high-frequency variability in the surface meteorology, with short-lived events at hourly and shorter time scales, and the relatively rapid, 1-min sampling captured peak winds as high as 23.1 m s^{-1}. At the same time, the low-frequency variability associated with the annual cycle and the transition between the seasons are evident (Fig. 10) in the low-passed surface meteorological data.

Air temperature was minimum in February–March and maximum in July. Wind direction shifted from the southeast quadrant (from westerlies to northerlies) in winter and spring, to the northeast quadrant (from southerlies to westerlies) in summer and fall. In summer, the Bermuda high anticyclone is well established, and

TABLE 6. Means, maxima, minima, and standard deviations of the basic meteorological observables computed from the hourly, 15-month file.

	Mean	Max	Min	Std dev
Wind speed (m s^{-1})	7.38	18.76	0.03	3.47
Wind direction (°)	85.2			
Air temperature (°C)	17.88	28.90	0.72	6.05
Sea temperature (°C)	21.10	28.91	6.75	4.67
Relative humidity (%)	77.3	99.6	43.0	11.0
Specific humidity (g k^{-1})	10.53	23.14	2.81	4.37
Barometric pressure (mb)	1015.5	1037.8	981.8	8.4
Incoming shortwave (W m^{-2})	133.0	974.9	0.0	219.9
Incoming longwave (W m^{-2})	355.8	447.4	226.9	42.1
Rain rate (mm h^{-1})	0.27	16.92	0.00	0.89

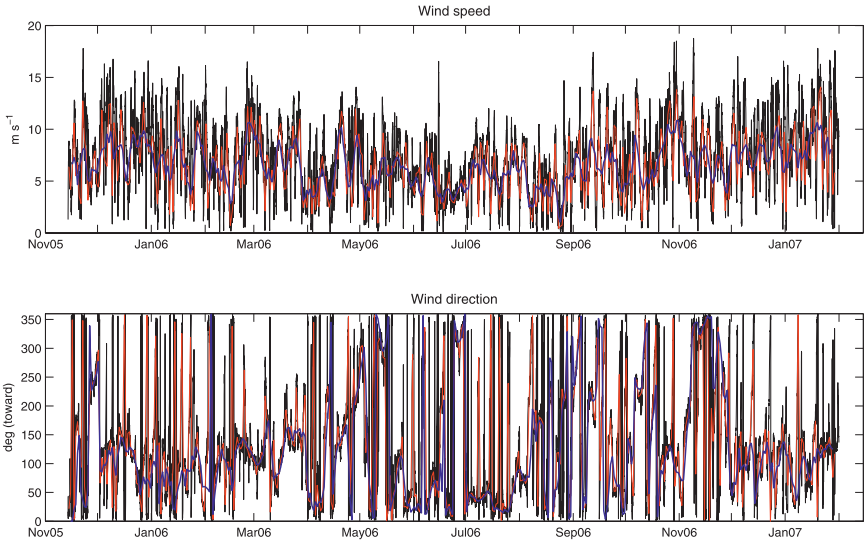

FIG. 9. Time series of (top) wind speed and (bottom) direction. Direction gives the direction toward which the wind flows. The hourly data are shown (black line). A 24-h running mean (red), and a 4-day boxcar average (blue) are also shown.

warmer, moister air, lower wind speeds, and less synoptic weather variability were seen. During the fall and winter, a number of strong wind events brought cold, dry air to the location.

c. *Bulk formula air–sea fluxes*

To complete the overview of the data, a summary of the bulk formula flux observations is presented. More discussion, including of the uncertainties and comparison with the DCFS fluxes, is provided in Part II. The mean meteorological data were used together with the Coupled Ocean–Atmosphere Response Experiment (COARE) 3.0 bulk algorithm (Fairall et al. 1996, 2003) to compute the wind stress τ, the latent heat flux Q_E, and the sensible heat flux Q_H. Net shortwave radiation Q_{SW} was determined from observed incoming solar radiation, using an albedo varying with sun elevation and atmospheric transmittance [empirical lookup tables from Payne (1972)] in the COARE algorithm. Net longwave radiation Q_{LW} was calculated from observed incoming longwave radiation by estimating the outgoing longwave radiation as $\varepsilon\sigma T^4$, where the emissivity ε was 0.97, σ was the Stefan–Boltzmann constant, and T was sea surface skin temperature (K). The surface current was approximated from the current meter measurement at 10 m and subtracted from the wind vector; the resultant relative wind was used in the COARE algorithm. Freshwater flux was computed using evaporation calculated from the latent heat flux and rain measurements.

Figure 11 shows the bulk formula fluxes computed from the mean meteorological data in Fig. 10. Table 6 and 7 show statistics for the daily values of bulk measurement and corresponding air–sea fluxes. The net heat flux shown by the second panel of Fig. 11 is determined from

$$Q_{\mathrm{net}} = Q_E + Q_H + Q_{\mathrm{SW}} + Q_{\mathrm{LW}} + Q_R,$$

where Q_R is the contribution to the sensible heat resulting from rain and the heat fluxes are defined as positive downward, that is, a positive value implies that

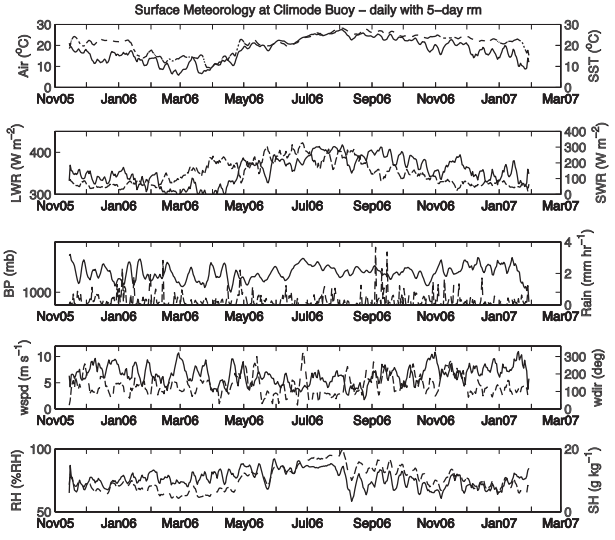

FIG. 10. An overview of the mean meteorological observations. All variables are 5-day running means of daily averages. For each plot, the *y* axis corresponding to the dashed line is to the right.

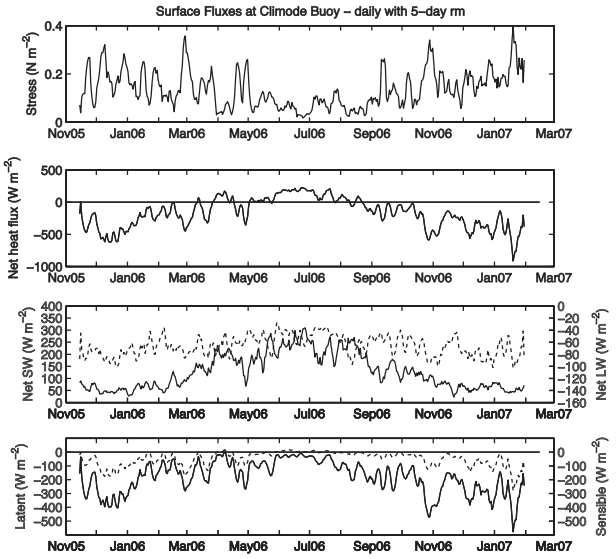

FIG. 11. Daily mean air–sea flux time series corresponding to Fig. 10.

the ocean is warming. The ocean lost heat to the atmosphere in the winter and gained heat in the summer with respective extrema in December and June. The shortwave radiative heat input was maximum in June. The largest component of heat loss occurred through latent heat exchange; sensible and net longwave radiative heat losses were secondary but nonnegligible, and similar in magnitude with each other on a monthly time scale, although the former was much stronger during synoptic events. All heat fluxes exhibited a similar annual cycle. During winter, strong latent heat loss contributed to large total heat loss by the ocean, with daily averages peaking at greater than 1000 W m^{-2}; in summer, under stronger solar radiation and reduced evaporation, the ocean gained heat. The flow of cold, dry air offshore during winter brought the largest heat losses, peaking at 1407 W m^{-2}.

5. Conclusions and discussion

We reported here the first long-term in situ observations of meteorological conditions near the sea surface in the Gulf Stream region. The surface mooring was successfully deployed for almost 15 months in the Gulf Stream region, which allowed for the continuous collection of upper-ocean and surface meteorological observations and the computation of the air–sea fluxes of heat, freshwater, and momentum. We did encounter challenges.

We believe that the surface mooring design, including the use of the fairing, was appropriate for the site and the conditions. The design tools we used were found to be applicable even in the Gulf Stream. The failure of the nylon line, and the suggestion that the failure was due to being cut rather than mechanical failure under load, does leave us concerned. Because the ability of the nylon to stretch as the drag forces mount is part of the reason why such moorings succeed in coping with high currents; we would not plan to replace the nylon with wire rope or more cut-resistant but less elastic material. The presence of ship traffic remains a concern, and redeployment in this location would use active radar transponders as well as passive radar reflectors. We would also consider the use of radio alerts to vessels coming within, say, 15 km of the surface buoy.

TABLE 7. Means, maxima, minima, and standard deviations of the basic fluxes computed using the bulk formula from observables the hourly, 15-month file.

	Mean	Max	Min	Std dev
Wind stress (N m^{-2})	0.152	1.357	0.000	0.158
Net heat flux (W m^{-2})	−170.5	832.8	−1407.9	337.5
Latent heat flux (W m^{-2})	−181.6	133.4	−834.0	150.4
Sensible heat flux (W m^{-2})	−50.3	111.2	−487.1	73.2
Net shortwave (W m^{-2})	127.6	925.4	0.0	208.0
Net longwave (W m^{-2})	−66.3	−7.1	−132.4	25.8
Freshwater flux (mm h^{-1})	0.04	3.39	−0.94	0.50

While the oceanographic instrument payload was limited by drag and mooring design constraints, we did succeed at obtaining near-surface currents and temperature and temperature–salinity data in the upper ocean that resolved the mixed layer depth over the year. The surface buoy payload was greater and this capacity was needed. Success at obtaining meteorological time series depends heavily on redundancy and robustness of the sensors. The propeller–vane anemometers have proven to be susceptible to damage, and sonic anemometers would be used instead. The use of three redundant sets of sensors was not overkill in this environment. Because of the redundancy, we only had to make limited use of other data to complete the 15-month time series of surface meteorology and support computation of the air–sea exchanges of heat, freshwater, and momentum for the length of the deployment.

Acknowledgments. This work was funded by the National Science Foundation Grant OCE04-24536 as part of the CLIVAR Mode Water Dynamics Experiment (CLIMODE). The Vetlesen Foundation is also acknowledged for the early support of SB. The design, fabrication, and deployment of a surface mooring in the Gulf Stream in November 2007, the recovery of that mooring in November 2008, and the deployment of the

second mooring in November 2008 were only possible through design assistance from Dr. Mark Grosenbaugh (WHOI) and the skill of the staff from the Upper Ocean Processes Group, the Mooring and Rigging Shop, the Mooring Operations Group, and the crew of R/V *Oceanus*. Thanks to Dr. Terry Joyce and the R/V *Knorr* for the recovery of the upper part of the second surface mooring in February 2007.

REFERENCES

Bower, A. S., and N. G. Hogg, 1996: Structure of the Gulf Stream and its recirculations at 55°W. *J. Phys. Oceanogr.,* **26,** 1002–1022.

Colbo, K., and R. A. Weller, 2009: The accuracy of the IMET sensor package in the subtropics. *J. Atmos. Oceanic Technol.,* **9,** 1867–1890.

Cronin, M. F., and Coauthors, 2010: Monitoring ocean–atmosphere interactions in western boundary current extensions. *Proc. OceanObs'09: Sustained Ocean Observations and Information for Society,* Vol. 2, ESA Publ. WPP-306, Venice, Italy, ESA. [Available online at https://abstracts.congrex.com/scripts/jmevent/abstracts/FCXNL-09A02a-1697411-1-Cronin-cwp2b01.pdf.]

Edson, J. B., A. A. Hinton, K. E. Prada, J. E. Hare, and C. W. Fairall, 1998: Direct covariance flux estimates from mobile platforms at sea. *J. Atmos. Oceanic Technol.,* **15,** 547–562.

Fairall, C. W., E. F. Bradley, D. P. Rogers, J. B. Edson, and G. S. Young, 1996: Bulk parameterization of air-sea fluxes in TOGA COARE. *J. Geophys. Res.,* **101** (C2) 3747–3767.

——, ——, J. E. Hare, A. A. Grachev, and J. B. Edson, 2003: Bulk parameterization of air–sea fluxes: Updates and verification for the COARE algorithm. *J. Climate,* **16,** 571–591.

Gobat, J., and M. Grosenbaugh, 2000: WHOI Cable v2.0: Time domain numerical simulation of moored and towed oceanographic systems. Woods Hole Oceanographic Institution Tech. Rep. WHOI-2000-08, 83 pp. [Available online at http://iop.apl.washington.edu/~jgobat/cable.pdf.]

Grosenbaugh, M. A., 1995: Designing oceanographic surface moorings to withstand fatigue. *J. Atmos. Oceanic Technol.,* **12,** 1101–1110.

Hosom, D. S., R. A. Weller, R. E. Payne, and K. E. Prada, 1995: The IMET (Improved Meteorology) ship and buoy systems. *J. Atmos. Oceanic Technol.,* **12,** 527–540.

Joyce, T. M., C. Wunsch, and S. D. Pierce, 1986: Synoptic Gulf Stream velocity profiles through simultaneous inversion of hydrographic and acoustic Doppler data. *J. Geophys. Res.,* **91** (C6), 7573–7585.

Konda, M., H. Ichikawa, H. Tomita, and M. F. Cronin, 2010: Surface heat flux variations across the Kuroshio as observed by surface flux buoys. *J. Climate,* **23,** 5206–5221.

Kubota, M., N. Iwabe, M. F. Cronin, and H. Tomita, 2008: Surface heat fluxes from the NCEP/NCAR and NCEP/DOE reanalyses at the Kuroshio Extension Observatory buoy site. *J. Geophys. Res.,* **113,** C02009, doi:10.1029/2007JC004338.

Larsen, S. E., J. B. Edson, C. W. Fairall, and P. G. Mestayer, 1993: Measurement of temperature spectra by a sonic anemometer. *J. Atmos. Oceanic Technol.,* **10,** 345–354.

Marshall, J., and Coauthors, 2009: Observing the cycle of convection and restratification over the Gulf Stream system and the subtropical gyre of the North Atlantic Ocean: Preliminary results from the CLIMODE field campaign. *Bull. Amer. Meteor. Soc.,* **90,** 1337–1350.

Meinen, C. S., D. S. Luther, and M. O. Baringer, 2009: Structure, transport and potential vorticity with the Gulf Stream at 68°W: Revisiting older data sets with new techniques. *Deep-Sea Res. I,* **56,** 41–60.

Miller, S. D., T. S. Hristov, J. B. Edson, and C. A. Friehe, 2008: Platform motion effects on measurements of turbulence and air–sea exchange over the open ocean. *J. Atmos. Oceanic Technol.,* **25,** 1683–1694.

Moore, G. W. K., and I. A. Renfrew, 2002: An assessment of the surface turbulent heat fluxes from the NCEP–NCAR reanalysis over the western boundary currents. *J. Climate,* **15,** 2020–2037.

Payne, R., 1972: Albedo of the sea surface. *J. Atmos. Sci.,* **29,** 959–970.

Rossby, T., and H.-M. Zhang, 2001: The near-surface velocity and potential vorticity structure if the Gulf Stream. *J. Mar. Res.,* **59,** 949–975.

Schulz, E. W., M. A. Grosenbaugh, L. Pender, D. J. M. Greenslade, and T. W. Trull, 2011: Mooring design using wave-state estimation from the Southern Ocean. *J. Atmos. Oceanic Technol.,* **28,** 1351–1360.

Shay, T. J., J. M. Bane, D. R. Watts, and K. L. Tracey, 1995: Gulf Stream flow field and events near 68°W. *J. Geophys. Res.,* **100** (C11), 22 565–22 589.

Tupper, G., S. Bigorre, and B. Weller, 2008: Making progress and wanting more: One-year near-surface current measurements from a surface mooring in the Gulf Stream and other thoughts about long-term surface moorings. *Proc. IEEE/OES/CMTC Ninth Working Conf. on Current Measurement Technology,* Charleston, South Carolina, IEEE, 111– 118, doi:10.1109/CCM.2008.4480852.

Weller, R. A., and S. P. Anderson, 1996: Surface meteorology and air–sea fluxes in the western tropical Pacific warm pool during the TOGA Coupled Ocean-Atmosphere Response Experiment. *J. Climate,* **9,** 1959–1990.

Yu, L., R. A. Weller, and B. Sun, 2004: Improving latent and sensible heat flux estimates for the Atlantic Ocean (1988-1999) by a synthesis approach. *J. Climate,* **17,** 373–393.